A RAIM APPROACH TO GNSS OUTLIER AND CYCLE SLIP DETECTION USING L1 CARRIER PHASE TIME-DIFFERENCES

M. Kirkko-Jaakkola[a], J. Traugott[b], D. Odijk[c], J. Collin[a], G. Sachs[b], and F. Holzapfel[b]

[a] Department of Computer Systems, Tampere University of Technology, Finland
[b] Institute of Flight System Dynamics, Technische Universität München, Germany
[c] Department of Spatial Sciences, Curtin University of Technology, Australia

ABSTRACT

Cycle slips are a common error source in Global Navigation Satellite System (GNSS) carrier phase measurements. In this paper, the cycle slip problem is approached using Receiver Autonomous Integrity Monitoring (RAIM) methodology. Carrier phase measurements are used here in a single-receiver time-differential positioning method where integer ambiguities are canceled, but any cycle slips remain. The performance of the method was assessed by comparing the detection results to a Real-Time Kinematic (RTK) solution and by manual data examination. Postprocessing results obtained using authentic Global Positioning System (GPS) measurements logged by low-cost single-frequency receivers show that the method is able to reliably detect and identify single errors but fails in an exemplary multiple outlier scenario. As no reference receiver is needed, the method is a potential means to produce cycle-slip-corrected data usable in any postprocessing application.

Index Terms— GNSS, carrier phase, cycle slip, RAIM, time-differential positioning

1. INTRODUCTION

The Global Navigation Satellite System (GNSS) carrier phase observable is a key to high positioning precision. Using it, however, is not straightforward as phase measurements are biased by *ambiguities*.[1] During continuous phase lock, the ambiguity remains constant, allowing for cancelation by subtracting two consecutive measurements. This is the key idea in time-differential (TD) positioning [1]. However, a temporary loss of phase lock may cause the ambiguity to change, resulting in a *cycle slip*. Time-differencing does not cancel cycle slips, so they must be detected as each slipped cycle corresponds, at the GPS L1 frequency, to 19 cm of range error which is much if decimeter-level or better precision is desired.

Cycle slip detection is typically based on geometry-free observables or measurement prediction. Canceling the range component requires either dual-frequency measurements or knowledge on the receiver dynamics from, e.g., inertial sensors [2]. However, these features increase hardware costs. Measurement prediction can be done by simple polynomial fitting or using, e.g., a Kalman filter. The wavelet transform has also been applied to cycle slip detection [3]. In a dynamic application the measurements may, however, be hard to predict or model with wavelets.

Receiver Autonomous Integrity Monitoring (RAIM) has been extensively researched and successfully used in traditional pseudorange-based GNSS positioning, but such a method has also been applied on carrier observables [4]. RAIM is based on measurement redundancy which poses a requirement of an overdetermined system of equations. The least-squares position solution residual can be used as a measure of consistency: if the norm of the residual exceeds some predefined threshold value, an alarm is raised. Further investigations can be made to pinpoint the faulty measurement.

The goal of this work is to use and to assess the performance of a RAIM method on cycle slip detection using standalone time-differenced data. The method could be used as a preprocessing step for any carrier phase processing application as no assumptions are made on, e.g., receiver dynamics.

2. CARRIER PHASE OBSERVABLE AND CYCLE SLIPPING

The GNSS carrier phase measurement for satellite S at epoch t_i can be modeled as

$$\Phi_i^S = \rho_i^S + c\delta_i^R - c\delta_i^S + T_i^S - I_i^S + \frac{\lambda}{2}N'^S + \epsilon_i^S \qquad (1)$$

where ρ_i^S is the distance between the receiver and satellite S. δ_i^R and δ_i^S denote the receiver and satellite clock biases, respectively, scaled to units of meters by the speed of light c. $T_i^S - I_i^S$ corresponds to atmospheric effects (tropospheric delay and ionospheric advance). N'^S is the ambiguity which is constant during continuous phase lock. λ denotes the carrier wavelength, and ϵ_i^S comprises modeling errors such as multipath, ephemeris errors, and measurement noise.

[1] The ambiguity is usually referred to as *integer ambiguity* as fractional components caused by satellite and receiver phase biases cancel (only) when forming *double* differences as required for RTK.

Even though the ambiguity is usually referred to in units of *full* carrier cycles, there may be an additional half-cycle ambiguity due to the navigation message modulated on the signal. As the message is not known beforehand, it cannot be removed to obtain a clean sinusoidal carrier wave to track. For this reason, carrier tracking loops are sometimes constructed as Costas loops which are insensitive to 180° phase shifts caused by, e.g., navigation data bit changes. Such a loop does not know if it is tracking the carrier correctly or off by 180 degrees [5]. The receiver can, however, resolve this ambiguity by examining the decoded navigation data bits, but if it, for some reason, fails to do so, the ambiguous part of the carrier phase measurement is $\frac{\lambda}{2}N'$ as in Eq. (1), while normally it is $\lambda N'$. For this paper, only Costas-type half-cycle-ambiguity receivers were used.

If the signal tracking is subject to a temporary (shorter than the sampling period) discontinuity, the ambiguity N'^S may change while the fractional part remains consistent, resulting in a cycle slip. Cycle slips are of persistent nature, i.e., the change in N'^S will affect all subsequent measurements to the same satellite as well. Due to the half-cycle ambiguity, the smallest possible cycle slip is $\pm\frac{1}{2}$ cycles, equivalent to approximately 10 cm at the L1 band. The receiver may also be, due to, e.g., multipath, subject to random-magnitude (no integer constraint) temporary measurement blunders, yielding *outlier* measurements. In the scope of this paper, detected errors are not categorized to slips and errors.

A new observable constructed by forming time differences of (1) is given by Eq. (2):

$$\begin{aligned} {}^{bi}\mathrm{D}\Phi^S &\overset{\text{def.}}{=} \Phi_i^S - \Phi_b^S \\ &= {}^{bi}\mathrm{D}\rho^S + c\,{}^{bi}\mathrm{D}\delta^R + \frac{\lambda}{2}\cancelto{0}{{}^{bi}\mathrm{D}N'^S} \\ &\quad + {}^{bi}\mathrm{D}\delta^S + {}^{bi}\mathrm{D}\left(T^S - I^S\right) + {}^{bi}\mathrm{D}\epsilon^S \end{aligned} \tag{2}$$

with ${}^{bi}\mathrm{D}$ denoting the time difference operator between epochs t_b and t_i. The major advantage of this observable is that the integer ambiguity term is canceled—but possible cycle slips and outliers are not. Moreover, atmospheric and other temporally correlated errors are reduced. The price is that uncorrelated errors (noise) are amplified $\sqrt{2}$-fold.

3. METHODS

3.1. Time-Differential Processing

Forming an observable as given in Eq. (2) allows ambiguity cancelation while utilizing precise L1 carrier-phase observations. This fact is taken advantage of to obtain high relative positioning precision when measuring dynamic trajectories using low-cost single frequency receivers. The core navigation algorithm to obtain the relative solution (base vector) between two epochs is based on an iterative least-squares (LS) solution of Eq.(3), similar to code-based single point positioning (no filtering applied).

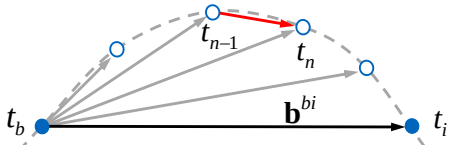

Fig. 1. Relative time-differential positioning. The initial position at t_b is known. The trajectory can be resolved either by accumulating the position increments (t_n, t_{n-1}) or from the over-all differences (t_i, t_b). In either case, the incremental solution is used for the presented RAIM method.

$$ {}^{bi}\mathrm{D}\widetilde{\boldsymbol{\Phi}} - {}^{bi}\mathrm{D}\widehat{\boldsymbol{\Phi}}\left(\boldsymbol{\xi}_{i,0}, \boldsymbol{\xi}_b\right) = \mathbf{H}_{\boldsymbol{\xi}_{i,0}}\Delta\boldsymbol{\xi}. \tag{3}$$

Here $\boldsymbol{\Phi} = \left(\Phi^1, \Phi^2, \ldots, \Phi^m\right)^T$ is the observation vector to all $m \geq 4$ satellites constantly tracked between t_b and t_i, and $\boldsymbol{\xi} = \left(x, y, z, c\delta^R\right)^T$ is the combined position and time solution which is assumed to be known for the base epoch $(\boldsymbol{\xi}_b)$ but unknown for the current time $(\boldsymbol{\xi}_i)$. The $\widetilde{}$ sign designates measurements while $\widehat{}$ represents modeled quantities. This (over-determined) set of equations once solved, the over-all trajectory can be reconstructed by either accumulating the position increments between subsequent epochs t_{n-1}, t_n or by directly forming over-all differences between the base epoch t_b and the current time t_i, compare Fig. 1. Each procedure has particular advantages and shortcomings which are out of this brief paper's scope.

Note that there is no need for a second, near-by base receiver and no (static) initialization as required by RTK approaches [6]. This advantage does not come for free. The remaining, non-modeled errors (compare last line of Eq.(2)) increase with increasing processing time causing a slow position drift. This fact limits possible processing intervals to a few minutes only. The drift can only be reduced by using external corrections. It cannot be avoided but it can be monitored and quantified. More details are given in [1, 7].

3.2. Receiver Autonomous Integrity Monitoring

As any cycle slips or outliers bias the time differences, they must be detected accordingly. In traditional pseudorange positioning, measurement blunders are usually screened out by means of a RAIM process.

The need for RAIM originates from civil aviation where measurement errors are uncommon but large (dozens or hundreds of meters) and caused by the space segment. In a safety-critical application such as aviation, the user cannot wait—possibly for hours—for the control segment to detect the satellite malfunction and to upload new satellite health data. Thus, the receiver must be able to autonomously detect biased measurements in order to meet required navigation

performance specifications. As the likelihood of a satellite failure is low, many RAIM schemes assume that no more than one error can occur at a time.

The original application of RAIM totally differs from the context of cycle slip detection where errors are small (even sub-meter), occur considerably often, and are caused by, e.g., receiver dynamics and environment, i.e., in the user segment. However, RAIM is based on measurement redundancy in least-squares estimation which is directly applicable on time-differential positioning.

RAIM is based on the assumption that a biased observation in the measurement set should not fit well in the others.The least-squares residual

$$\mathbf{f} = \widetilde{\mathbf{y}} - \widehat{\mathbf{y}} = \widetilde{\mathbf{y}} - \mathbf{H}\widehat{\mathbf{x}} = \widetilde{\mathbf{y}} - \mathbf{H}\left(\mathbf{H}^T\mathbf{H}\right)^{-1}\mathbf{H}^T\widetilde{\mathbf{y}}, \quad (4)$$

with $\mathbf{H}$ denoting the (linearized) measurement model and $\widetilde{\mathbf{y}}$ being the observed measurements, can be used as a measure of inconsistency. According to [8], an outlier alert is issued if the condition

$$\|\mathbf{f}\| > T_D; \quad \text{with} \quad T_D = f\left(P_{\text{FA}}, \sigma, m\right) \quad (5)$$

holds. The test statistic $\|\mathbf{f}\|$ is χ^2 distributed with $m-4$ degrees of freedom. Consequently, T_D has to be calculated from the inverse χ^2 cumulative density function corresponding to the expected range measurement noise σ and the number of used satellites m for a user-defined false alarm rate P_{FA}. T_D, as given by [8], for code noise typical at the time and a rather strict false alarm probability as suggested by RTCA is shown in the left-hand side plot of Fig. 2. This value is due to the civil aviation background of RAIM, and is not applicable for cycle slip detection for reasons described above.

Typically, the RAIM procedure is followed by computation of the protection level, i.e., the largest position error that may occur unnoticed with the current RAIM parameters. This is not, however, of much interest at cycle slip detection.

3.3. Detection and Exclusion Procedure using Time-Differences

Within this first approach, the goal of time-difference integrity monitoring is limited to outlier detection and exclusion. When using accumulated position increments for reconstructing the over-all trajectory, see Fig. 1, there is no need for cycle slip and outlier discrimination or even cycle slip repair, as each incremental solution is independent from previous measurements. This is the main benefit of the accumulation strategy. Hence, the latter issues are only marginally addressed in the remainder of this article whilst the focus is put on the exclusion task. Instead of $\|\mathbf{f}\|$ as proposed by [8], the test statistic RMS $(\mathbf{f})$ as defined by (6) and (7) is used.

$$\text{RMS}\left(\mathbf{f}\right) = \sqrt{\frac{\sum_{i=1}^{m} f^{i\,2}}{m-1}} = \frac{\|\mathbf{f}\|}{\sqrt{m-1}} \quad (6)$$

$$f^i = {}^{n-1,n}\text{D}\widetilde{\Phi}^i - {}^{n-1,n}\text{D}\widehat{\Phi}^i \quad (7)$$

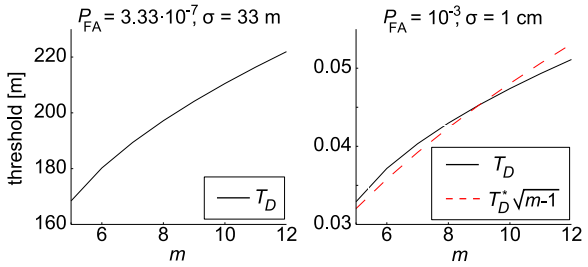

Fig. 2. Outlier detection threshold vs. number of satellites. *Left*: Threshold as initially proposed by [8] when using $\|\mathbf{f}\|$ as test statistic for code measurements with standard deviation as high as 33 m and a false-alarm rate $3.33 \cdot 10^{-7}$.
Right: Threshold according to [8] and the effective threshold from Eq. (9) (using $T_D^* = 1.6$ cm) with noise and false-alarm settings appropriate for carrier phase time-differences.

Here subsequent epochs (t_{n-1}, t_n), spanning intervals between 0.1 and 1 second only depending on the receiver's measurement rate settings, are used. The effect of drifting errors virtually vanishes for such short time spans causing the residual level to be very low (in the millimeter range). Hence outliers generate distinct spikes in the test statistic. Note that this would not hold when using over-all differences (t_i, t_b) for outlier detection, as the residual level increases with increasing drift of non-modeled errors. The corresponding decision rule is stated in Eq. (8):

$$\text{RMS}\left(\mathbf{f}\right) > T_D^* = \text{constant} \quad (8)$$

$$\|\mathbf{f}\| > T_D^*\sqrt{m-1} \quad (9)$$

Here T_D^* is independent of the number of satellites m. However the effective threshold for $\|\mathbf{f}\|$ (i.e. if $\|\mathbf{f}\|$ was chosen as test statistic instead of RMS $(\mathbf{f})$) does adapt to m, Eq. (9). As shown by the right-hand side plot of Fig. 2, this adaption is only off by less than 5 % from the threshold values proposed by [8] for typical time-difference applications—if T_D^* is set 'smartly'. Smartly means: (1) Choose an appropriate false alarm rate, e.g. 0.1 % for not-safety-critical applications. (2) Determine the expected measurement noise. This can be done by empirical experience with the used equipment or by using the variance estimate as dropping out of the least-squares solver: $\sigma_{\text{D}\widetilde{\Phi}} = (\sum f^2/(m-4))^{1/2}$. A phase noise standard deviation of 1 cm is typical for low-cost receivers in dynamic applications. (3) Determine a typical number of satellites of the data to be processed, e.g. 9. (4) Get T_D from the inverse χ^2 cumulative density function for the chosen values (here 5 d.o.f.). (5) Calculate T_D^*. This done, a detection and exclusion logic as outlined by Fig. 3 can be executed.

Resting upon redundancy information out of the over-determined set of navigation equations (Eq. 3), the test statistic will always be bound to virtually zero for only 4 satellites in view. Consequently, outlier detection is impossible for

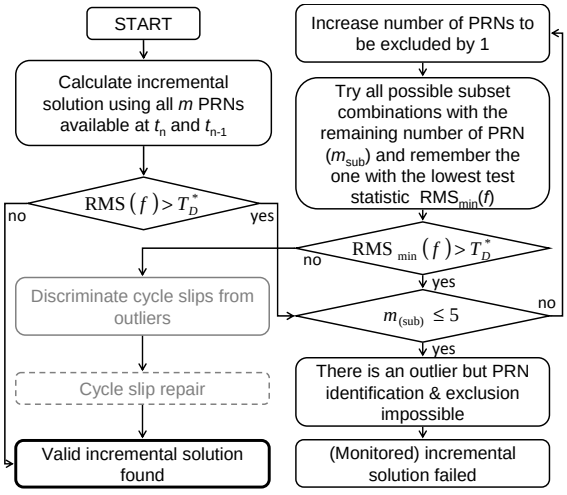

Fig. 3. Outlier detection and exclusion algorithm. Cycle slip discrimination and repairing make more measurements usable but are not addressed in the scope of this paper.

the 4-in-view case and exclusion is only feasible for more than 5 used satellites. This problem is common to all RAIM approaches. The outlier search strategy as proposed in Fig. 3 causes a high computational load, especially in multiple-outlier scenarios. This impedes the application of the method in real-time applications. Moreover, most RAIM schemes are based on a single-outlier assumption which does not hold in the context of cycle slip detection. Hence RMS $(\mathbf{f})$ alone may not be ideally suited as test statistic for the multiple outlier case, and alternative methods, as proposed by e.g. [9], may achieve better results. As mentioned in Sec. 2, cycle slips bias all subsequent epochs whereas outliers only afflict individual observations. As residuals of $(n-1, n)$-time-differences (Eq. (7)) are the basis for outlier detection, a single error at, say, t_n, always afflicts ${}^{n-1,n}\mathrm{D}\widetilde{\Phi}^i$ and ${}^{n,n+1}\mathrm{D}\widetilde{\Phi}^i$ with an offset of similar absolute value but opposite sign. This can cause the erroneous exclusion of the respective PRN at t_{n+1}.

The proposed approach is a true snap-shot method not using information from previous or subsequent measurements. It further provides the option for outlier and cycle slip discrimination by analyzing the residuals of excluded satellites. Residuals which are (close to) an integer multiple of $\frac{\lambda}{2}$ (or λ for full-cycle-ambiguity receivers) indicate the presence of a slip. Merging this information with the opposite sign characteristic of outliers in the residual history is regarded as a means to address the discrimination and even repair task.

4. PERFORMANCE TESTING

The method was tested using various sets of authentic GPS data, all logged for post-processing by low-cost u-Blox L1-only GPS receivers capable of raw-data sampling rates up to 10 Hz. During the first flight test, a stationary base receiver was available for RTK computations. Precise ephemerides, clock corrections, and ionosphere data were used.

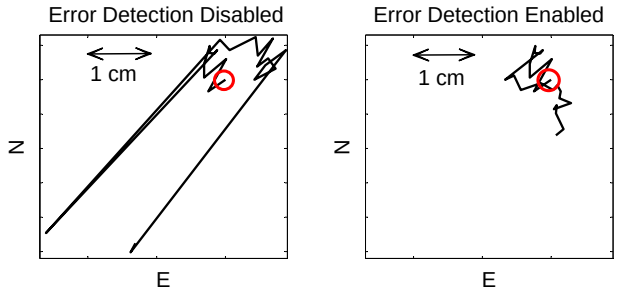

Fig. 4. Static data: Analysis in position domain. East and North components of the resulting trajectory with and without outlier detection. The initial location is marked with a circle.

4.1. Static Test

The static test was expected to be an easy starting point for validating the correctness of the theory. Stationary receivers are less prone to cycle slips than moving ones and the presence of an outlier is easy to observe from the solution trajectory as it should not contain distinctive jumps. Fig. 4 demonstrates the effect of outliers in the position domain and the top plot of Fig. 5 shows the corresponding test statistic values. The processed interval was short, only 22 seconds, but contained two measurement errors, both on the same satellite (PRN 4), which are well visible in the trajectory computed without error detection. 9 satellites were available, and only the remaining 8 were used after the outlier was detected.

The pattern of the residuals as depicted in the second plot of Fig. 5 reveals a magnitude of $\frac{\lambda}{2}$ of the measurement errors proposing the presence of half-cycle slips. However, two subsequent epochs are affected in the first case. This indicates the presence of a simple outlier instead of a slip impeding a concluding discrimination. For validation purposes, the non-differenced observations of PRN 4 were interpolated using cubic smoothing splines yielding residuals with a standard deviation similar to the one expected for the range measurements. The excluded measurements were not used when fitting. The fit residuals (bottom plot of Fig. 5) confirm the outlier hypothesis in the first case. In the second case the error is very small which prevents a solid discrimination.

4.2. Flight Test #1: Comparison With RTK

A kinematic test was performed using a data set measured during a test flight starting from Oberpfaffenhofen, Germany. The data begins with a 15-minute stationary section to facilitate RTK integer ambiguity resolution, followed by a flight containing circle and dynamic-soaring-like maneuvers. As

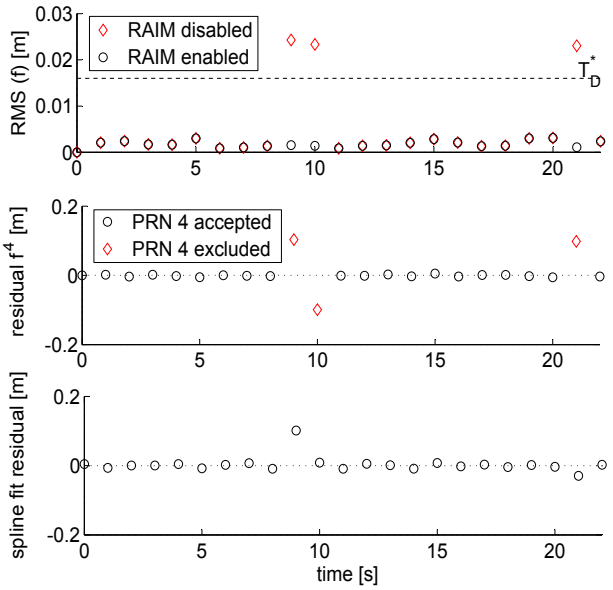

Fig. 5. Static data: Residual analysis.
Top: Test statistic with and without biased measurements.
Middle: Residuals of PRN 4, which is excluded by RAIM.
Bottom: Carrier phases for PRN 4 subtracted from a smoothing spline. Excluded measurements not used in spline fitting.

opposed to TD processing, RTK is unaffected by error drift but requires two receivers and an initialization to work [6].

The cycle slip detection results of the time-differential solution were compared to those derived from an RTK solution computed at Delft University of Technology, the Netherlands. A total of 165 errors, classified as cycle slips and outliers, were listed in the reference. The time-differential method detected 127 uncategorized errors. For the epochs where the TD method identified an error, time differences of the carrier phase measurements for the suspected satellite were examined to see if an error really had occurred or not. Table 1 shows how many detections were observed to be correct, wrong, or, as was the case for most epochs, uncertain due to, e.g., gaps in the phase data or, more frequently, nonuniform sampling of the phase measurements. The data was logged at 4 Hz but the measurement instants were not spaced by exactly 0.250 seconds. Instead, the measurement timestamps had second fractions .247, .499, .747, and .999. Time-differencing such data yields oscillatory results as every other measurement interval is slightly longer than the others, making visual inspection of the presence of cycle slips difficult, especially if the data originates from a highly dynamic scenario—as was the case. A resampling software was not used to mitigate the zigzag effect.

The detection results of the two methods were not even expected to be identical. Firstly, the RTK solution did not report any half-cycle slips which was due to the software not being configured to do so. However, the time-differential method did detect some half-cycle slips. Secondly, RTK solutions are computed from double-differenced data which causes cycle slips from both the rover and reference receivers to be subtracted from each other. Thus, a slip detected in RTK can have occurred in either of the two receivers. Even though the rover receiver is more prone to cycle slipping, several RTK detections were observed to have occurred in the reference receiver.

Table 1. Comparison of TD and RTK error detection results verified using raw phase data. The figures show how many of the detections were confirmed to be correct or wrong, and at how many epochs the data was not smooth enough for manual examination.

Detection results	TD Right	TD Wrong	Uncertain
Methods Agree	6	3	20
Methods Disagree	9	8	30
TD Detection only	2	4	31

In the verifiable cases, the methods achieved a similar performance: supposing that RTK was right in cases where the TD method was verified to be wrong and the methods disagreed, both methods were right in about 50 % of the verifiable epochs. Knowing that the flight data was highly dynamic and frequently suffered from a low number of visible satellites, this may be regarded as a fairly good performance, but cannot be considered conclusive.

4.3. Flight Test #2: Simultaneous Errors

As a real-life application, the time-differential method was used for estimating the takeoff and landing distances of the Mü30 "Schlacro" aircraft of AKAFLIEG München. The measurement process was repeated six times. During the landings, the aircraft bounced remarkably after hitting the ground, resulting in excessive losses of lock. One landing measurement is taken here to show the behavior of the presented method in the case of multiple simultaneous errors.

The reconstructed altitude profile is drawn in Fig. 6. The zoomed version shows an abrupt jump of about 20 cm in the altitude. That section was processed continuously with carrier phases and as the data was logged at 10 Hz, it is not a plausible explanation that the dynamics would have changed suddenly. At the epoch of interest, two cycle slips were detected. It is suspected that these identifications are incorrect.

Fig. 7 shows the time-differenced carrier phases for the used satellites, revealing three half-cycle slips. The error detection algorithm identified satellites 21 and 22 as faulty, but as it can be seen in the figure, PRN 22 is healthy. Thus, two of the remaining cycle slips remain undetected. Forcing PRN 21 to be totally excluded from the computations did not help: a false solution fits well enough in the measurement subset containing two biased measurements, and thus the exclusion al-

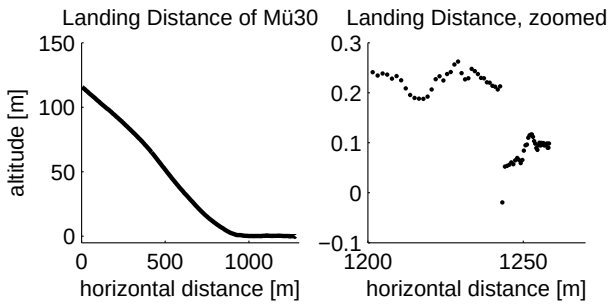

Fig. 6. Altitude profile of the aircraft landing measurement.

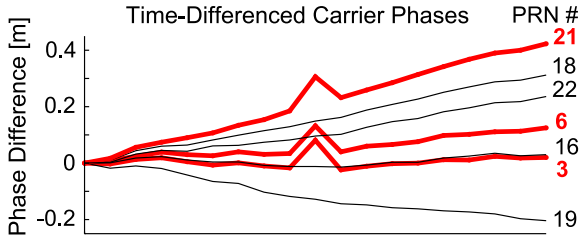

Fig. 7. Differences of consecutive carrier phases in the landing data. All lines have been shifted to begin at 0.

gorithm terminates after finding two satellites to be excluded. Therefore, the least-squares residual itself is not a sufficient quantity for detecting multiple simultaneous cycle slips in this case, which agrees with the single-outlier assumption in most RAIM schemes mentioned in the above.

5. CONCLUSIONS AND OUTLOOK

In this paper, the problem of cycle slipping was tackled by means of RAIM. The results show that despite the totally different origin, RAIM can detect even small single cycle slips and outliers in carrier phase data. Similar promising results have been observed in other tests [10].

As time-differential positioning and the presented outlier detection approach are relatively simple and easy-to-apply in the field procedures, they can be well used in not-safety-critical applications. Moreover, with an effective discrimination between outliers and cycle slips, the detected cycle slips could be corrected for and the method could be used as a preprocessing step for other phase processing methods. As future work, the performance with multiple simultaneous errors is to be further investigated.

6. ACKNOWLEDGEMENTS

The authors would like to acknowledge Dr. Oliver Montenbruck, DLR Germany, for strongly supporting the work on the time-differential approach.

7. REFERENCES

[1] J. Traugott, D. Odijk, O. Montenbruck, G. Sachs, and C. Tiberius, "Making a Difference with GPS," *GPS World*, vol. 19, no. 5, May 2008.

[2] K. de Jong, "Real-time integrity monitoring, ambiguity resolution and kinematic positioning with GPS," in *Proc. of the 2nd European Symposium on Global Navigation Satellite Systems*, October 1998.

[3] L. Gun, H. Yong-hui, and Z. Wei, "A New Algorithm of Detecting and Correction Cycle Slips in Dual-Frequency GPS," in *Proc. of the IEEE Intl. Frequency Control Symposium and Exposition*, June 2006.

[4] D. Odijk and S. Verhagen, "Recursive Detection, Identification and Adaptation of Model Errors for Reliable High-Precision GNSS Positioning and Attitude Determination," in *3rd Intl. Conference on Recent Advances in Space Technologies*, June 2007.

[5] E. Kaplan and C. Hegarty, *Understanding GPS Principles and Applications*, Artech House, 2nd edition, 2006.

[6] D. Odijk, J. Traugott, G. Sachs, O. Montenbruck, and C. Tiberius, "Two Approaches to Precise Kinematic GPS Positioning with Miniaturized L1 Receivers," in *Proc. of the 20th Intl. Technical Meeting of the Satellite Division of the Inst. of Navigation*, September 2007.

[7] J. Traugott, G. Dell'Omo, A.L. Vyssotski, D. Odijk, and G. Sachs, "A Time-Relative Approach for Precise Positioning with a Miniaturized L1 GPS Logger," in *Proc. of the 21st Intl. Technical Meeting of the Satellite Division of the Inst. of Navigation*, September 2008.

[8] R.G. Brown and G.Y. Chin, "GPS RAIM: Calculation of Threshold and Protection Radius Using Chi-Square Methods—A Geometric Approach," *Global Positioning System: Inst. of Navigation*, vol. V, 1997.

[9] S. Hewitson and J. Wang, "GNSS Receiver Autonomous Integrity Monitoring (RAIM) for Multiple Outliers," *The European Journal of Navigation*, vol. 4, no. 4, 2006.

[10] J. Traugott, "Measuring the dynamic soaring of albatrosses by time-differential processing of phase measurements from miniaturized L1 GPS receivers," Presentation at the Colloquium of Satellite Navigation of Technische Universtät München, June 2009, `http://www.nav.ei.tum.de` → Colloquium → Summer Term 2009.